A data-driven study of Alzheimer's disease related amyloid and tau pathology progression

Leon M. Aksman,[1,2] Neil P. Oxtoby,[3] Marzia A. Scelsi,[2] Peter A. Wijeratne,[3] Alexandra L. Young,[4,3] Isadora Lopes Alves,[5] Lyduine E. Collij,[6,7] Jacob W. Vogel,[8,9] Frederik Barkhof,[2,5,6] Daniel C. Alexander[3] and Andre Altmann[2] for the ADNI

Abstract

Amyloid-beta is thought to facilitate the spread of tau throughout the neocortex in Alzheimer's disease, though how this occurs is not well understood. This is because of the spatial discordance between amyloid-beta, which accumulates in the neocortex, and tau, which accumulates in the medial temporal lobe during aging. There is evidence that in some cases amyloid-beta-independent tau spreads beyond the medial temporal lobe where it may interact with neocortical amyloid-beta. This suggests that there may be multiple distinct spatiotemporal subtypes of Alzheimer's-related protein aggregation, with potentially different demographic and genetic risk profiles. We investigated this hypothesis, applying data-driven disease progression subtyping models to post-mortem neuropathology and in vivo PET based measures from two large observational studies: the Alzheimer's Disease Neuroimaging Initiative and the Religious Orders Study and Rush Memory and Aging Project.

We consistently identified 'amyloid-first' and 'tau-first' subtypes using cross-sectional information from both studies. In the amyloid-first subtype, extensive neocortical amyloid-beta precedes the spread of tau beyond the medial temporal lobe, while in the tau-first subtype mild tau accumulates in medial temporal and neocortical areas prior to interacting with amyloid-beta. As expected, we found a higher prevalence of the amyloid-first subtype among apolipoprotein E (APOE) ε4 allele carriers while the tau-first subtype was more common among APOE ε4 non-carriers. Within tau-first APOE ε4 carriers, we found an increased rate of amyloid-beta accumulation (via longitudinal amyloid PET), suggesting that this rare group may belong within the Alzheimer's disease continuum. We also found that tau-first APOE ε4 carriers had several fewer years of education than other groups, suggesting a role for modifiable risk factors in facilitating amyloid-beta-independent tau. Tau-first APOE ε4 non-carriers, in contrast,

recapitulated many of the features of Primary Age-related Tauopathy. The rate of longitudinal amyloid-beta and tau accumulation (both measured via PET) within this group did not differ from normal aging, supporting the distinction of Primary Age-related Tauopathy from Alzheimer's disease. We also found reduced longitudinal subtype consistency within tau-first APOE ε4 non-carriers, suggesting additional heterogeneity within this group.

Our findings support the idea that amyloid-beta and tau may begin as independent processes in spatially disconnected regions, with widespread neocortical tau resulting from the local interaction of amyloid-beta and tau. The site of this interaction may be subtype-dependent: medial temporal lobe in amyloid-first, neocortex in tau-first. These insights into the dynamics of amyloid-beta and tau may inform research and clinical trials that target these pathologies.

Author affiliations:

1 Stevens Neuroimaging and Informatics Institute, Keck School of Medicine, University of Southern California, CA, 90033, USA

2 Centre for Medical Image Computing, Department of Medical Physics and Biomedical Engineering, University College London, London, WC1V 6LJ, UK

3 Centre for Medical Image Computing, Department of Computer Science, University College London, London, WC1V 6LJ, UK

4 Department of Neuroimaging, Institute of Psychiatry, Psychology and Neuroscience, King's College London, London, SE5 8AF, UK

5 Brain Research Center, 1081 GN Amsterdam, The Netherlands

6 Department of Radiology and Nuclear Medicine, Amsterdam UMC, Vrije Universiteit Amsterdam, PO Box 7057, 1007MB, Amsterdam, The Netherlands

7 Amsterdam Neuroscience, Brain Imaging, De Boelelaan 1085, 1081 HV Amsterdam, The Netherlands

8 Department of Psychiatry, University of Pennsylvania, Philadelphia, PA, 19104, USA

9 Lifespan Informatics and Neuroimaging Center, University of Pennsylvania, Philadelphia, PA, 19104 , USA

Correspondence to: Leon Aksman, PhD

Stevens Hall for Neuroimaging

2025 Zonal Avenue

Los Angeles, CA 90033

USA

E-mail: leon.aksman@loni.usc.edu

Running title: Data-driven amyloid and tau subtypes

Keywords: Alzheimer's disease; PART; data-driven subtyping; PET imaging; neuropathology

Abbreviations: AD = Alzheimer's disease; ADNI = Alzheimer's Disease Neuroimaging Initiative; Aβ = amyloid-β; APOE = apolipoprotein E; CN = cognitively normal; CVIC = cross-validation information criterion; KDE = kernel density estimation; MTL = medial temporal lobe; MCI = mild cognitive impairment; NFTs = neurofibrillary tangles; PART = primary age-related tauopathy; PVD = positional variance diagram; RADC = Rush Alzheimer's Disease Center; ROSMAP = Religious Orders Study and Rush Memory and Aging Project; SuStaIn = Subtype and Stage Inference; SUVR = standardized update value ratio

Introduction

Alzheimer's disease (AD) is a progressive neurodegenerative disease that is characterized at the molecular level by the accumulation of two specific protein-based pathologies within the brain: amyloid plaques, composed of extracellular amyloid-β (Aβ) peptide, and intracellular

neurofibrillary tangles (NFTs), composed of abnormally hyperphosphorylated tau protein. These pathologies combine to create a toxic environment that drives neurodegeneration via neuronal and synaptic loss, leading to cognitive impairment.[1] While Aβ and tau have been recognized as the primary signature of AD, the causal relationship between these two pathologies is not fully understood. The prevailing view set forth by the amyloid cascade hypothesis is that the accumulation of Aβ peptides is the main causative event triggering the pathogenesis of AD, with tau-based NFTs, neurodegeneration and cognitive impairment following as a result.[2,3]

Importantly, the amyloid cascade hypothesis does not require that Aβ occurs first in all AD cases. Tau-based NFTs are well known to accumulate within the medial temporal lobe (MTL; includes entorhinal cortex, hippocampus and amygdala) in most individuals by their fifth or sixth decade in an age-related process that is independent of Aβ.[4,5] Therefore, rather than occurring first, Aβ is thought to facilitate the spread of tau beyond the MTL.[6] How this occurs is not well understood due to the spatial disconnection between Aβ accumulation, which usually begins in the parietal, cingulate and frontal regions in the neocortex,[7,8] and age-related tau accumulation in the MTL.[9] These pathologies may initiate independently and only interact when Aβ eventually spreads to the MTL. It is also possible that tau in the MTL somehow initiates neocortical Aβ,[10] although a recent study in genetically identical twins supports the causal effect of Aβ on tau rather than the opposite.[11] A third possibility is that tau spreads beyond the MTL in some cases[12] and may interact locally with neocortical Aβ, which then amplifies tau. Taken together, these possibilities suggest that there may be two basic subtypes of pathology progression in AD: an 'amyloid-first' variant, in which widespread Aβ plaques precede neocortical NFTs, and a 'tau-first' variant, in which early neocortical NFTs precede widespread Aβ.

In this study we set out to investigate the existence of multiple spatiotemporal patterns of Aβ and tau progression using *in vivo* PET from the Alzheimer's Disease Neuroimaging Initiative (ADNI) and postmortem neuropathologic measures from the Religious Orders Study and Rush Memory and Aging Project studies (ROSMAP). We employed a data-driven paradigm to uncover subtypes of pathologic progression using the SuStaIn (Subtype and Stage Inference) algorithm.[13] SuStaIn identifies groups of participants with common patterns of disease progression from multi-modal cross-sectional data. It has previously been used to establish the existence of multiple subtypes of both Aβ and tau spread.[8,14] We consistently identified 'amyloid-first' and 'tau-first'

progression patterns, each of which is marked by a distinct spatiotemporal pattern of Aβ and tau spreading. We then tested for differences in demographic and apolipoprotein E (APOE) ε4 status between these subtypes to better understand their relationship to AD and primary age-related tauopathy (PART[15]), the latter being characterized by age-related tau in the MTL in the absence of Aβ. Finally, using longitudinal Aβ and tau PET and cognition in ADNI, we investigated the longitudinal consistency of the PET-based subtyping model and tested for differences in the rates of Aβ and tau accumulation and cognitive decline between subtypes stratified by APOE ε4 status.

Materials and methods

ROSMAP dataset

We used postmortem neuropathology data from the Religious Orders Study (ROS) and Rush Memory and Aging Project (MAP) studies, collectively referred to as ROSMAP, which we obtained from the Rush Alzheimer's Disease Center (RADC).[16] Participants in these studies are cognitively normal (CN) older adults who agree to annual evaluations and organ donation as a condition of study entry. We used molecularly-specific immunohistochemistry based measures of Aβ protein (percent area of region occupied) and neuronal neurofibrillary tangles (associated with abnormally phosphorylated tau protein; cortical density per mm^2 measured via AT8 staining**)** both measured in eight brain regions: hippocampus, entorhinal cortex, midfrontal cortex, inferior temporal cortex, angular gyrus, calcarine cortex, anterior cingulate cortex and superior frontal cortex. We also used demographic information (age at death, sex, education years), final (*in vivo*) clinical diagnosis of AD (NINCDS-ARDRA[17]), (postmortem) neuropathologic diagnosis of AD (NIA-Reagan Criteria[18]), CERAD score (a semiquantitative measure of neuritic plaques[19]) and Braak stage (a semiquantitative measure of the distribution and severity of NFTs[20]).

ADNI dataset

Data used in the preparation of this article were obtained from the Alzheimer's Disease Neuroimaging Initiative (ADNI) database (adni.loni.usc.edu). The ADNI was launched in 2003 as

a public-private partnership, led by Principal Investigator Michael W. Weiner, MD. The primary goal of ADNI has been to test whether serial magnetic resonance imaging (MRI), positron emission tomography (PET), other biological markers, and clinical and neuropsychological assessment can be combined to measure the progression of mild cognitive impairment (MCI) and early Alzheimer's disease (AD). For up-to-date information, see www.adni-info.org.

We downloaded and collated spreadsheets with imaging, demographic, cognitive and cerebrospinal fluid (CSF) measures from the ADNI IDA website. We downloaded regional amyloid PET (18F-AV-45, florbetapir) standardized update value ratios (SUVRs; `UCBERKELEYAV45_8mm_02_17_23.csv`) as well as both the standard regional tau PET (18F-AV-1451, flortaucipir) SUVRs (`UCBERKELEYAV1451_8mm_02_17_23.csv`) and partial volume corrected regional tau PET SUVRs (`UCBERKELEYAV1451_PVC_8mm_02_17_23.csv`). We also downloaded the ADNIMERGE table, containing demographic information (age, sex, years of education, number of APOE ε4 alleles), and diagnostic labels (CN/MCI/AD). We downloaded composite measures of memory (ADNI-MEM[21]) and executive function (ADNI-EF[22]) both available in `UWNPSYCHSUM_12_13_21.csv`. We download the following CSF spreadsheets: `UPENNBIOMK9_04_19_17.csv` (ADNI1/GO/2 Aβ-42, pTau, tTau), `UPENNBIOMK10_07_29_19.csv` (ADNI3 Aβ-42, Aβ-40, pTau, tTau), `UPENNBIOMK12_01_04_21.csv` (additional ADNI3 Aβ-42, Aβ-40, pTau, tTau). The ADNI database was last accessed on March 24th, 2023.

Disease progression modeling

We used SuStaIn, a probabilistic machine learning method, to characterize the heterogeneity of Aβ and tau pathology progression in AD. SuStaIn infers multiple patterns of disease progression (i.e. subtypes) as well as individuals' disease stages from cross-sectional data.[13] The SuStaIn model as introduced by Young et al.[13] uses a data likelihood based on how far a biomarker measurement deviates from normality, with an associated set of *z*-score based events for each biomarker. Note that in biomarkers where controls have very little abnormality, the resulting *z*-scores in patients can become large owing to the small amount of variance in the control population. This is indeed the case when modeling the progression of PET-based SUVRs, where

the variability of the PET signal in the control group (e.g. Aβ load in CN APOE ε4 negative participants, representing normal aging) can be quite small. We therefore followed the approach taken by Vogel et al.[14] in our PET-based analysis, defining three events for each regional SUVR: $z = 2$, 5 and 10. These correspond roughly to mild, moderate and severe abnormality relative to the control group.

For our neuropathology-based analysis, we used an extension of SuStaIn (Ordinal SuStaIn[23]), that is adapted to handle severity scores from neuropathology rather than continuous values. This model was recently applied to model the progression of TDP-43 pathology using regional neuropathological severity score ratings, with each region assigned a score ranging from 0 (non-detectable) to 3 (severe).[24] Because we did not have regional scores we estimated them by combining the quantitative, immunohistochemistry-based measures of pathology (Aβ and tau tangle severity in eight regions, described above) with CERAD scores for overall neuritic plaque burden (neuritic plaques are composed of insoluble Aβ) and Braak stages for overall NFT severity and spatial extent. We fit a kernel density estimation (KDE) based probability distribution to the quantitative pathology measures associated with each CERAD or Braak score (or grouping of scores) and used a mixture-model based approach to assign a severity score probability to each individual in each region.

To do this we used the following procedure: for a set of regions $i = 1, \dots, I$, participants $j = 1, \dots, J$ and unique severity scores $k = 1, \dots, K$, we fit a KDE-based probability distribution $p(x|\text{score} = k, \text{region} = i)$ to describe the probability of a pathology measure x in region i given score k, resulting in a mixture of K distributions per region. We performed the KDE mixture modeling in Python, using the `gaussian_kde` function in scikit-learn. In total we fit $I * K$ distributions for all regions and severity scores. Following mixture modeling, we calculated $p(\text{score}_{i,j,k})$, the probability of severity score k in region i for a given participant j with pathology measure m_{ij} as:

$$p(\text{score}_{i,j,k}) = \frac{p(m_{ij}|\text{score} = k, \text{region} = i)}{\sum_{k'=1}^{K} p(m_{ij}|\text{score} = k', \text{region} = i)}$$

where the numerator is the probability of observing the pathology measure under the probability distribution for score k in region i. The denominator assures that the severity score probabilities add up to one for each participant in each region.

We applied the above procedure to the set of Aβ measures and CERAD-based scores to generate a subjects-by-regions-by-scores matrix of severity score probabilities for regional Aβ severity. We applied the same procedure to the set of tau tangle measures and Braak-based scores to generate a second matrix of severity score probabilities for regional tau severity.

We used the pySuStaIn software package[25] for both the PET-based *z*-score SuStaIn analysis and the neuropathology-based Ordinal SuStaIn analysis. In both cases we optimized the number of subtypes in an iterative manner using ten-fold cross-validation. Following previous SuStaIn-based studies,[13,14] we evaluated the cross-validation information criterion (CVIC; described in Young et al.[13]). We chose the number of subtypes that consistently minimized the CVIC across both analyses.

ROSMAP subtyping

The ROSMAP study is an ongoing observational study of older adults that have agreed to annual clinical evaluation and cognitive testing as well as brain donation after death. Through 2022 there were 3,751 participants enrolled, with 1,853 deaths. There were a total of 1,338 participants who had a complete set of Aβ and NFT measures for all eight available brain regions (hippocampus, entorhinal cortex, midfrontal cortex, inferior temporal, angular gyrus, calcarine cortex, anterior cingulate cortex, superior frontal cortex).

In order to run SuStaIn on these participants, we first took the square root of each measure to improve normality and then corrected each measure for the effect of normal aging and normal demographic differences by training a region-specific regression model on a control population with the measure in question as the dependent variable and age at death, sex and education years as the independent variables. The control population consisted of 145 APOE ε4 negative (ε4-) CN participants (based on a summary diagnostic opinion regarding most likely clinical diagnosis at time of death) with a CERAD score of 'no AD', indicating very low or no neuritic plaques. We

then residualized each region (true value minus predicted value from regression) and used these residualized measures in the mixture modeling procedure described above to estimate the regional score probability matrices for both Aβ and tau tangle pathologies.

For estimating regional Aβ score probabilities we combined the regional Aβ measures with the global CERAD score that was available for each participant. The CERAD score has four possible values: 'no AD', 'possible AD', 'probable AD' and 'definite AD'. We used these directly to create four distributions for each region. For estimating regional tau tangle score probabilities we combined the regional NFT measures with each participant's Braak stage, which ranges from 0 (no NFTs), I and II (initial NFTs in entorhinal and early hippocampal regions), III and IV (worsening in previous regions and spread throughout temporal and cingulate regions) and V and VI (worsening in previous regions and spread to remaining cortex)[20]. In this case, to maintain consistency with the four Aβ severity scores, we grouped some Braak stages together, creating four tau severity scores. For the entorhinal and hippocampus regions the groups were: Braak 0/I/II (reflecting normal age-related tau in the MTL in those over 75[4]), Braak III/IV (mild), Braak V (moderate) and Braak VI (severe). For the other six regions, which become abnormal in later Braak stages (cingulate, calcarine, angular gyrus, inferior temporal, midfrontal, superior frontal) the groups were: Braak 0/I/II/III (none or minimal), Braak IV (mild), Braak V (moderate) and Braak VI (severe). We then followed the mixture modeling procedure with four severity scores for both Aβ and tau pathologies, generating a regional severity score probability matrix that were then combined and input to Ordinal SuStaIn.

ADNI subtyping

We performed SuStaIn-based analyses using cross-sectional PET data from ADNI. We used ten regional amyloid PET (AV-45) SUVRs and twelve tau PET (AV-1451) SUVRs, many of which were composites of several Freesurfer-based SUVRs (for complete details see Supplementary Table 1).[26,27] We formed composite regions using volume-weighted averaging of two or more adjacent regions. We excluded the hippocampal tau PET SUVR as this region is suspected to be contaminated by off-target binding in the choroid plexus.[28] We reference normalized all SUVRs as recommended for cross-sectional analysis: for amyloid PET we used a

reference region made up of the whole cerebellum; for tau PET we used the inferior cerebellum in our main analysis and the inferior cerebellar grey matter for partial-volume corrected SUVRs for our supplementary analysis.[29,30] For longitudinal analysis of Aβ and tau accumulation, we used the same reference region for tau PET and the recommended composite region (unweighted average of whole cerebellum, brainstem/pons and subcortical white matter) for amyloid PET.[29]

As in the ROSMAP analysis, we removed the associations with normal aging and normal demographic factors by training a regression model for each biomarker's values against age, sex and education years in a control population of 49 CN participants who were APOE ε4-, global amyloid SUVR negative (whole cerebellum normalized summary SUVR < 1.11 cut-off[31,32]) and CSF Aβ negative (Aβ-42/Aβ-40 ratio > 0.06 cut-off[33]). We then regressed out the signal due to these factors from all markers. There were a total of 1,645 participants with either amyloid PET or tau PET scans at a single visit, of which 796 had only amyloid PET and 327 had only tau PET. We built the main *z*-score SuStaIn model using the 502 participants who had complete concurrent amyloid and tau PET imaging. These were 47 CN, 406 with mild cognitive impairment (MCI) and 49 AD participants. To test the robustness of our main model, we used the same set of participants and trained an additional SuStaIn model with the same ten amyloid PET SUVRs and partial volume corrected tau PET SUVRs for the same twelve composite regions.

We assessed the longitudinal consistency of the ADNI subtyping model using 170 participants who had concurrent amyloid and tau PET imaging at one or more follow-up visits. There were 210 follow-up samples in total: 22 at one-year follow-up, 103 at two-year follow-up, 13 at three-year follow-up, 57 at four-year follow-up, ten at five-year follow-up and five at six-year follow-up. We created confusion matrices for subtype consistency within the APOE ε4- and ε4+ groups using the 103 participants with two year follow-up (58 ε4-, 45 ε4+).

Statistical comparisons of early-stage groups

Following SuStaIn modeling, we tested for genetic and demographic differences between the stage-zero group (those assigned stage zero in either subtype, representing normal aging) and those in the early stages of the amyloid-first and tau-first groups that we identified in both analyses. These early-stage groups included participants with abnormality in either Aβ or tau but not both

at the same time to avoid the scenario in which SuStaIn cannot reliably disambiguate between subtypes based on a patients' cross-sectional biomarker pattern. We stratified both the early amyloid-first and early tau-first groups by APOE ε4 carriage (ε4- versus ε4+) and tested for differences in Aβ and tau pathology across the five groups. For the neuropathology analysis, we tested for differences in Aβ in the angular gyrus and midfrontal regions (two of the earliest regions to show abnormality in our model) and for differences in tau tangles in the entorhinal cortex and hippocampus (two early Braak stage regions). For the PET analysis we tested for differences in Aβ pathology in the global amyloid SUVR and CSF Aβ-42/Aβ-40 ratio; for tau we tested for differences in the tau PET entorhinal regional SUVR. We also test for differences in CSF pTau. In each case we tested for differences across the five groups using three linear regressions, each time setting the regional measure as the dependent variable and sex, education years and group coding variables as the independent variables. In each case the first model included all groups, testing for differences relative to the stage zero reference group. The second model tested for differences within the two early amyloid-first groups (ε4+ vs. ε4-). The third similarly tested for differences within the two early tau-first groups.

We then tested for demographic and genetic differences across these groups. We tested for differences in the proportion of early amyloid-first, early tau-first and stage-zero groups within APOE ε4- and ε4+ participants using a chi-squared test. As before, we tested for differences in age across the five groups using three linear regressions, each time setting age as the dependent variable and sex, education years and group coding variables as the independent variables. We tested for differences in sex using a set of three logistic regressions, each time setting sex as the dependent variable and age, education years and group coding variables as the independent variables. Finally, we tested for differences in education using a set of three linear regressions with education as the dependent variable and age, sex and group coding as the independent variables.

We investigated group differences in the rates of longitudinal Aβ and tau accumulation and cognitive decline using a set of linear mixed effects models (LMEs). All LME models were fitted using the *fitlme* function in Matlab (R2023a) with default parameters: using maximum likelihood with a full covariance matrix using Cholesky parameterization. For ROSMAP we modeled ante-mortem cognitive decline using all available longitudinal measures of global cognition, which is a composite measure of 19 cognitive tests that has been previously described by Bennet *et al.*[34] For

ADNI we modeled Aβ and tau accumulation using amyloid PET and tau PET measures and cognitive decline using composite memory score (ADNI-MEM) and composite executive function (ADNI-EF). For these models we used samples from all available visits (i.e. including visits that were both prospective and retrospective to the PET visit used in SuStaIn modeling) and used stage-zero (ε4-) participants as the reference group. For amyloid and tau PET we trained an LME model with fixed effects of baseline age, sex, education years, intracranial volume (ICV), time (years since baseline) and time × subtype interaction and individual-level random intercepts and random slopes with time. For the cognition models in ROSMAP and ADNI we used these same LME fixed and random effects, excluding ICV.

Data availability

ROSMAP data can be requested at: https://www.radc.rush.edu, ADNI data is publicly available at: https://adni.loni.usc.edu and pySuStaIn is freely available at https://github.com/ucl-pond/pySuStaIn. Analysis code used in this study is available upon reasonable request.

Results

Demographics for the ROSMAP and ADNI cohorts used in our subtyping analyses are shown in Table 1. ROSMAP participants were older than ADNI participants (ROSMAP: 89.9 $\pm$ 6.4, ADNI: 75.2 $\pm$ 7.9 years; $P < 10^{-6}$) while ADNI participants had more years of education (ROSMAP: 15.9 $\pm$ 3.6, ADNI: 16.4 $\pm$ 2.6 years; $P = 0.005$). ROSMAP had a higher proportion of females (ROSMAP: 69%, ADNI: 50%; $P < 10^{-6}$) while ADNI had a higher proportion of APOE ε4 carriers (ROSMAP: 76%/22%/2% (0/1/2 alleles), ADNI: 65%/28%/7% (0/1/2 alleles); $P < 10^{-6}$).

Amyloid-first and tau-first subtypes

Supplementary Figure 1 depicts the mixture models that were fit for the ROSMAP analysis. We used these models to generate the regional severity score probability matrices, which were combined and input to Ordinal SuStaIn. Supplementary Figure 2 depicts the distribution of *z*-

scores for CN, MCI and AD participants' SUVRs in ADNI, showing that CN and MCI participants' *z*-scores are generally small (with higher variability of scores within the MCI group) and AD participants' *z*-scores are substantially higher, as expected. We used these *z*-scores as input to *z*-score SuStaIn.

We estimated the number of subtypes that best explain the progression of Aβ and tau pathology in both datasets. To do this we built separate SuStaIn models for each dataset, allowing SuStaIn to infer one, two, or three-subtype models in each case and we chose the most parsimonious models across both datasets. Supplementary Figure 3 depicts the cross-validation information criterion (CVIC; lower is better) for both datasets. We chose the two-subtype models for all subsequent analyses as there was a consistent improvement over a one-subtype model in both analyses.

Based on the two-subtype models we chose, Figure 1 depicts the positional variance diagrams (PVDs) representing the progression patterns estimated by SuStaIn. Each PVD visualizes event sequence uncertainties as a matrix where each row presents a set of three histograms, one per event, that are represented by colored boxes. In both analysis, each region has three stages of increasing abnormality relative to a control group that is expected to be at minimal risk of AD (in both cases: amyloid-negative, APOE ε4-, CN participants).

Across both analyses we consistently found an 'amyloid-first' and a 'tau-first' subtype. In the neuropathology analysis, the 'amyloid-first' subtype is characterized by the initial spread of Aβ plaques throughout the cortex and MTL (here represented by the hippocampus and entorhinal cortex). Following severe Aβ plaques in all regions, mild tau tangle pathology in the hippocampus and entorhinal cortex (exceeding Braak I/II severity expected in normal aging) spreads to the inferior temporal lobe and throughout the neocortex (Figure 1A). The latter stages of this subtype are marked by increasing tau tangle pathology, which progresses from mild to moderate to severe. The 'tau-first' subtype is characterized initially by mild tau tangle pathology in the entorhinal cortex, hippocampus, inferior temporal lobe and cingulate. Mild tau in these regions is followed by the spread of Aβ plaques throughout the brain, with subsequent increase in tau tangle pathology throughout the MTL and neocortex (Figure 1B).

In the PET-based analysis the 'amyloid-first' subtype is initially marked by the spread of Aβ that progresses to a severity that is at least five standard deviations from normality in all

regions. Following this, mild tau accumulates in the entorhinal cortex and amygdala (beyond what is expected in normal aging, with hippocampus excluded in this analysis) and spreads throughout the cortex, with increased severity of both Aβ and tau pathologies (Figure 1C). The 'tau-first' subtype is marked by mild tau abnormality in all regions (*z*-scores of two in frontal, temporal, parietal, occipital and cingulate regions), followed by the spread of Aβ throughout the cortex (up to a *z*-score of five in most regions) with subsequent increased tau severity in all regions (Figure 1D).

We built several additional SuStaIn-based subtyping models to test the robustness of our findings. The first two were based on the CVIC figure in Supplementary Figure 3, which showed a slightly lower CVIC for a three-subtype model rather than a two-subtype in the case of the PET-based analysis. For the sake of completeness we present the three-subtype model for both datasets in Supplementary Figures 5 and 6. Increasing to three subtypes consistently creates an additional 'tau-first' subtype in which tau in the MTL (entorhinal cortex and hippocampus in the neuropathology model, entorhinal cortex and amygdala in the PET-based model) precedes Aβ. The third model substituted partial volume corrected tau PET SUVRs in place of standard SUVRs in the PET-based model. Supplementary Figure 7 presents this model, which is very similar to the main PET-based model presented in Figure 1C, 1D.

Amyloid and tau differences among early stage groups

For the neuropathology model we defined the early amyloid-first group as those with moderately abnormal Aβ and no abnormal tau (stages one through 16 in Figure 1A, $n = 168$; APOE ε4-: 135, APOE ε4+: 33) and the early tau-first group as those with mild tau and no abnormal Aβ (stages one through four in Figure 1B, $n = 151$; ε4-: 142, ε4+: 9). The stage zero group was composed of $n = 106$ participants in this case. For the PET-based model the early amyloid-first group was defined as those with $z = 2$ level abnormality in most regional amyloid PET SUVRs and no abnormal tau (stages one through nine in Figure 1C, $n = 87$; APOE ε4-: 50, APOE ε+: 37) and the early tau-first group as those with $z = 2$ level abnormality in nearly all tau PET SUVRS and no abnormal Aβ (stages one through nine in Figure 1D, $n = 72$; APOE ε4-: 62, APOE ε+: 10). The stage zero group was composed of $n = 120$ participants in this case.

For the neuropathology model we found the expected increase in Aβ in the angular gyrus and mid frontal regions within both early amyloid-first groups relative to the stage-zero group (ε4-: angular gyrus $t = 14.4$, $P < 10^{-6}$, midfrontal $t = 12.3$, $P < 10^{-6}$; ε4+ angular gyrus t = 11.6, $P < 10^{-6}$; midfrontal t = 8.4, $P < 10^{-6}$; Figures 2A and 2B). Similarly, we found increased tau tangles in the entorhinal cortex and hippocampus in both early tau-first groups relative to the stage-zero group (ε4-: entorhinal cortex $t = 15.1$, $P < 10^{-6}$, hippocampus $t = 13.1$, $P < 10^{-6}$; ε4+: entorhinal cortex $t = 5.1$, $P < 10^{-6}$, hippocampus $t = 6.4$, $P < 10^{-6}$; Figures 2C and 2D). We also found a small increase in tau tangles in the hippocampus in the early amyloid-first group (ε4-) relative to the stage-zero group ($t = 2.1$, $P = 0.04$; Figure 2D).

For the PET-based model we found the expected increase in global amyloid PET SUVR within both early amyloid-first groups relative to the stage-zero group (ε4-: $t = 16.1$, $P < 10^{-6}$, ε4+: 14.5, $P < 10^{-6}$; Figure 2E). We also found a small increase in global amyloid PET SUVR in the early tau-first group (ε4-) versus the stage-zero group ($t = 5.3$, $P < 10^{-6}$; Figure 2E). We found decreased CSF Aβ-42/Aβ-40 ratio (indicative of increased Aβ deposition) in the early amyloid-first (ε4+) group relative to both the early amyloid-first (ε4-) group and the stage-zero group (ε4+ vs stage-zero: $t = -5.0$, $P < 10^{-6}$; ε4+ vs. ε4-: $t = -3.0$, $P = 0.006$; Figure 2F). We also found the expected increase in entorhinal region tau PET SUVR signal in both early tau-first groups relative to the stage-zero group (ε4-: $t = 7.2$, $P < 10^{-6}$; ε4+: $t = 4.8$, $P = 2.8 \times 10^{-6}$; Figure 2G). Finally we found a small increase in CSF pTau in the early amyloid-first (ε4+) group relative to the stage-zero group ($t = 2.0$, $P = 0.04$; Figure 2H).

Higher proportion of early amyloid-first group within APOE ε4 carriers

We consistently found that APOE ε4+ participants were more likely to belong to the early amyloid-first group than ε4- participants (neuropathology model: 69% of ε4+ in early amyloid-first group versus 36% of ε4- participants, chi-squared = 19.3, $P = 6.3 \times 10^{-5}$; PET-based model: 57% ε4+ versus 23% ε4-, chi-squared = 26.2, $P = 2.0 \times 10^{-6}$; Figures 3D and 3H). Within the neuropathology model we also found a higher proportion of females in the early amyloid-first (ε4-) group than in the stage-zero group (early amyloid-first, ε4- group: 76% female, stage-zero group:

52% female, odds ratio: 2.8, $P = 3.4\times10^{-4}$, Figure 3B) and a small increase in years of education in the early amyloid-first (ε4+) group compared to the early amyloid-first (ε4-) group (Mean ± SD: 17.4 ± 4.3 years versus 16.4 ± 3.8 years; $t = 2.5$, $P = 0.01$, Figure 3C). Within the PET-based model we found those in the early tau-first (ε4-) group were slightly older and more likely to be female than those in the stage-zero group (age: 76.9 ± 7.4 years versus 73.4 ± 7.7 years, $t = 3.6$, $P = 4.1\times10^{-4}$, Figure 3E; sex: 55% female versus 40% female, odds ratio: 2.4, $P = 0.01$; Figures 3E and 3F). Those in the early tau-first (ε4+) group were also more likely to be female compared to those in the stage-zero group (80% versus 40%, odds ratio: 5.4, $P = 0.04$; Figure 3F). In addition, those in the early tau-first (ε4+) group had fewer years of education than both the early tau-first (ε4-) group and the stage-zero group (ε4+: 14.7 ± 3.8 years, ε4-: 16.9 ± 2.5 years, stage-zero: 16.8 ± 2.6 years; ε4+ versus ε4-: $t = -2.1$, $P = 0.04$; ε4+ versus stage-zero: $t = -2.2$, $P = 0.03$).

Longitudinal consistency of tau-first subtype depends on APOE ε4 status

We visualized the longitudinal consistency of the PET-based model with spaghetti plots of all available follow-up samples, showing the expected increase in stage over time in the majority of participants (Figures 4A and 4C). Within the 103 participants with two-year follow-up, we found no difference in the annual rate of stage increase between subtypes in either ε4- or ε4+ participants (ε4-, $n = 58$: amyloid-first: 0.6 ± 2.1 stages/year, tau-first: 0.9 ± 3.9 stages/year, one-way ANOVA $P = 0.75$; ε4+, $n = 45$: amyloid-first: 0.8 ± 2.7 stages/year, tau-first: 0.9 ± 2.7 stages/year, $P = 0.87$). Within ε4- participants, the tau-first group had a lower two-year longitudinal consistency than the amyloid-first group (amyloid-first: 25 out of 27, 93%; tau-first: 8 out of 16, 50%; Figure 4B; Fisher's exact test $P = 0.003$). There was no such difference within ε4+ participants, where the two-year longitudinal consistency was high for both subtypes (amyloid-first: 25 out of 31, 81%; tau-first: 10 out of 11, 91%; Figure 4D, $P = 0.65$).

Amyloid accumulation within tau-first subtype depends on APOE ε4 status

Figure 5A depicts longitudinal trajectories of Aβ accumulation across early-stage groups from the PET-based model. We found increased intercepts and rates of amyloid accumulation within both early amyloid-first groups relative to stage-zero (ε4-: intercept $t = 2.6$, $P = 8.74 \times 10^{-3}$, group-by-time interaction: $t = 3.9$, $P = 8.79 \times 10^{-5}$; ε4+: intercept $t = 5.7$, $P < 10^{-6}$, group-by-time interaction: $t = 5.0$, $P < 10^{-6}$; Supplementary Table 3a). While these findings were expected for these groups, we also found an increased intercept and rate of Aβ accumulation within the early tau-first (ε4+) group, though longitudinal information was limited for this group ($n = 7$; intercept $t = 2.0$, $P = 0.04$, group-by-time interaction: $t = 3.4$, $P = 6.26 \times 10^{-4}$; Supplementary Table 3a). We found no corresponding increase in Aβ accumulation within the early tau-first (ε4-) relative to stage-zero ($n = 31$; Supplementary Table 3a).

Figures 5B-D depict longitudinal trajectories of tau accumulation within composite Braak regions. We found increased intercepts for both early tau-first groups within all three composite regions relative to the stage-zero group (Braak I, ε4-: $t = 2.7$, $P = 6.65 \times 10^{-3}$, ε4+: $t = 3.6$, $P = 3.44 \times 10^{-4}$; Braak III/IV, ε4-: $t = 8.0$, $P < 10^{-6}$, ε4+: $t = 3.8$, $P = 1.50 \times 10^{-4}$; Braak V/VI, ε4-: $t = 10.4$, $P < 10^{-6}$, ε4+: $t = 4.2$, $P = 3.18 \times 10^{-5}$; Supplementary Tables 3b-d). We found no corresponding differences in the rates of tau accumulation within these regions in either early tau-first group, suggesting that these groups have a high baseline level of tau but do not accumulate tau any faster than normal.

The early amyloid-first (ε4+) group was the only group in which we found increased tau accumulation, within both the Braak I and Braak III/IV composite regions (Braak I: $t = 4.1$, $P = 4.71 \times 10^{-5}$; Braak III/IV: $t = 2.3$, $P = 0.02$; Supplementary Tables 3b, 3c). We found no corresponding differences in intercepts in these regions within this group, suggesting that this group begins accumulating tau at an abnormally fast rate following widespread Aβ. We also found a small increase in intercept in the amyloid-first (ε4-) group within the Braak V/VI region, but no corresponding increase in the rate of tau accumulation (Braak V/VI: $t = 2.4$, $P = 0.02$), which may be due to additional heterogeneity within the ε4- group that is not well explained by our two-subtype model.

Finally, we found no differences in the rates of ante-mortem global cognitive decline in any of the four early-stage groups relative to the stage-zero group within our neuropathology dataset (Supplementary Table 4a; Supplementary Figure 4A). Within ADNI (PET-based model) we similarly found no increased rates of memory or executive function decline across early-stage groups and only a small difference in executive function intercept in the early tau-first (ε4+) group relative to the stage-zero group (t = -2.1, P = 0.04; Supplementary Table 4b, 4c; Supplementary Figure 4B, 4C).

Discussion

While Aβ and tau have long been established as the main pathological hallmarks of AD, the heterogeneity within the spatiotemporal progression of these pathologies has yet to be fully understood. Here we performed data-driven modeling on two large cohorts with complementary *in vivo* and postmortem measures, consistently finding 'amyloid-first' and 'tau-first' subtypes across both studies (Figure 1). In the 'amyloid-first' subtype, widespread Aβ throughout the neocortex and the MTL precedes neocortical tau. This supports the idea that a spatially and temporally localized interaction between Aβ and age-related tau in the MTL (Figure 2C, 2D) may trigger the spread of tau beyond the MTL (Figure 1A, 1C). The 'tau-first' subtype is marked by mild tau in the MTL and, in some cases, the neocortex (cingulate and inferior temporal lobe in the neuropathology-based model; all available cortical regions in PET-based model) preceding Aβ (Figure 1B, 1D). This finding supports *in vivo* tau PET studies,[12,35,36] neuropathology studies[37,38] and a recent combined study[39] which have found that mild tau may spread beyond the MTL in the presence of little or no Aβ. Our findings suggest that, in both subtypes, substantial neocortical tau accumulation may only occur after local interactions with Aβ. Importantly, the site of these interactions may differ between subtypes: in the amyloid-first subtype it occurs in the MTL (around stage 25 in Figure 1A and stage 23 in Figure 1C) while in the tau-first subtype it may occur in one or more neocortical regions where early Aβ deposition takes place (frontal, parietal or cingulate regions; around stage 5 in Figure 1B and around stage 13 in Figure 1D).

Beyond identifying these subtypes across complementary studies, our most important findings relate to their interaction with APOE ε4 status. Comparing the early stages of both

subtypes, we found a higher prevalence of the amyloid-first subtype among ε4 carriers and, conversely, a higher prevalence of the tau-first subtype among ε4 non-carriers (Figure 3D, 3H). Within the amyloid-first subtype, we found that ε4 carriers had greater Aβ deposition than ε4 non-carriers (lower Aβ-42/Aβ-40 ratio, Figure 2F). These findings are consistent with studies showing that APOE ε4 carriage is associated with increased Aβ deposition[40,41] and a higher lifetime risk of developing AD dementia.[42,43] Although we expected earlier Aβ deposition in ε4 carriers versus non-carriers,[44] we did not observe this in the PET-based analysis (Figure 3E). This may be because our criteria for defining the early amyloid-first groups was based on most regions having the mildest Aβ accumulation (*z*-scores of two in most amyloid SUVRs), which may have been reached many years before our study baseline (average age of participants in PET-based analysis was 75.2 ± 7.9 years; Table 1).[44] Consistent with this interpretation, we found both a higher baseline level and rate of Aβ accumulation in the early amyloid-first ε4 carriers compared non-carriers (Supplementary Table 3a).

Within the tau-first subtype we found an increased rate of Aβ accumulation in ε4 carriers compared to our normal aging reference group, suggesting that this rare group may belong within the AD continuum (9 out of 1,338 participants in neuropathology dataset: 0.7%; 10 out of 502 participants in ADNI: 2%; similarly infrequent in previous studies[45,46]). Interestingly, we found that those in the early tau-first (ε4+) group had several fewer years of education than other early-stage groups (Figure 3G). This suggests a role for modifiable risk factors, such as reduced years of education[47] or possibly head injury,[48] in facilitating Aβ-independent neocortical tau in those who would normally develop neocortical tau only after substantial Aβ accumulation.

The tau-first (ε4-) group recapitulates key features of PART, which is characterized by tau pathology in the absence of Aβ plaques.[15,49,50] The rate of both Aβ and tau accumulation within this group did not differ from normal aging despite increased baseline tau in both the MTL and neocortex (Figure 5 and Supplementary Table 3). Together with the older average age of this group (Figure 3E), this suggests a very slow process of tau accumulation over a number of years, beginning in middle age or even earlier.[4,51] This makes it hard to determine the exact sequence of progression of amyloid-independent tau. While our findings suggests that PART may be more closely related to normal aging than AD, our conclusions are tempered by our finding that the tau-first (ε4-) group had substantially lower longitudinal subtype consistency than other groups (Figure

4). The explanation for this may be that some of those who start out with mild tau in the MTL and/or neocortex and no Aβ subsequently develop low levels of Aβ, leading our model to misclassify their follow-up measures. These findings raise the question of whether: (i) the tau-first (ε4-) group represents PART, which is itself naturally heterogeneous and includes the roughly 30% of ε4 non-carriers who develop low levels of Aβ by their eight decade;[44] or (ii) those with PART are somehow protected from Aβ and therefore the tau-first (ε4-) group includes both PART and those on a slow trajectory of Aβ accumulation. These observations, which support several recent studies,[52,39] motivate the need to identify and track early tau-first, ε4 non-carriers to better understand the heterogeneity within this group.

Our tau PET sample is insufficient to validate the four PET-based tau subtypes found by Vogel, et al. based on a larger sample size of 1,143 tau PET images.[14] However, our findings may help to explain some of the tau heterogeneity in those who are Aβ positive.[53] Notably, the limbic-predominant subtype, which is characterized by Braak-like tau progression, has been found to have a higher proportion of APOE ε4 carriers. This is consistent with ε4 carriers having an earlier age of Aβ accumulation[44] and therefore we expect the amyloid-first (ε4+) group to be primarily composed of the limbic-predominant subtype. Interestingly, increased Aβ deposition within amyloid-first ε4 carriers relative to non-carriers (Figure 2F) may be related to the increased severity of MTL tangles within the limbic-predominant subtype. Correspondingly, we expect the amyloid-first (ε4-) group to be mostly composed of the other known tau subtypes (MTL-sparing, posterior and lateral temporal[14]). Importantly, once Aβ takes off we expect that it accelerates the spread of tau in all scenarios, consistent with the Aβ cascade hypothesis. The resulting picture is one of a slow tau accumulation process that is accelerated following local interaction with Aβ. The age and location at which this interaction takes place may depend on both genetic and modifiable risk factors of Aβ accumulation.[51] The spatial variability in how tau spreads may also depend on these factors plus individual-level and population-level factors.[54] Within this model, APOE ε4 non-carriers with PART are either partially or completely protected from Aβ while a small number of APOE ε4 carriers will develop abnormal tau prior to Aβ, possibly due to modifiable risk factors. While this model is probably an oversimplification it may be useful for future studies.

Our study has several important limitations. The first relates to the current lack of sufficiently long follow-up measures in the ADNI3 data, which may be remedied in ADNI4.[55]

This limited our validation of subtype consistency, which is important when using the Subtype and Stage Inference (SuStaIn) algorithm to infer longitudinal progression patterns from cross-sectional observations. This is because there is a theoretical possibility of inferring a progression pattern from a set of unrelated disease states. A related methodological limitation is the crossing problem, in which two or more subtypes have middle stages that look identical (e.g. an individual with mild tau plus Aβ may belong to either subtype). In our study we accounted for this problem by focusing on the early stages of each subtype. A version of SuStaIn that is explicitly longitudinally consistent, so that each individual is guaranteed to be assigned to the same subtype over multiple observations, is being developed to address these limitations[56]. There are also limitations related to comparing neuropathological measures from ROSMAP with *in vivo* measures from ADNI. The eight regional measures of Aβ and tau tangles measures used in neuropathological model were not anatomically consistent with the PET-based regional SUVRs, limiting our comparison of spatial progression patterns. This is especially evident in the tau-first subtype, where the lack of neuropathological measures in the precuneus, inferior frontal and orbitofrontal regions limited our ability to validate the PET-based finding that these may be among the earliest sites of tau and Aβ interaction (rather than the MTL in the amyloid-first subtype). We were also limited in our ability to fully characterize the heterogeneity within the tau-first APOE ε4 non-carrier group. Lastly, there were differences in age, education and sex across the ROSMAP and ADNI cohorts that limited our comparisons (Table 1).

In summary, in this study we identified amyloid-first and tau-first patterns of Aβ and tau accumulation using cross-sectional information from *in vivo* and postmortem data. We found increased Aβ accumulation within the amyloid-first subtype in both ε4-carriers and non-carriers. This supports the idea that both amyloid-first groups belong within the AD continuum. Using longitudinal amyloid PET, we found that those in amyloid-first (ε4+) group most likely develop Aβ at an earlier age than those in the amyloid-first (ε4-) group, recapitulating previous findings. Within the tau-first subtype, we found important differences when stratifying by APOE ε4 status. The first is that tau-first ε4-carriers probably belong in the AD continuum based on their increased Aβ accumulation, although this group is rare and so has limited longitudinal data. The overwhelming majority of those who develop AD are amyloid-first. The second is that tau-first ε4-noncarriers represent PART or are a mixture of PART plus those who accumulate Aβ very slowly. Our findings support the idea that the substantial neocortical tau that is observed in AD

may result from a local interaction of a slow, age-related tau accumulation process with Aβ. The timing and location of this interaction may be modulated by genetic and modifiable risk factors. These insights into the dynamics of Aβ and tau accumulation may inform research and clinical trials that target these pathologies.

Acknowledgements

Data used in preparation of this article were obtained from the Alzheimer's Disease Neuroimaging Initiative (ADNI) database (adni.loni.usc.edu). As such, the investigators within the ADNI contributed to the design and implementation of ADNI and/or provided data but did not participate in analysis or writing of this report. A complete listing of ADNI investigators can be found at: http://adni.loni.usc.edu/wp-content/uploads/how_to_apply/ADNI_Acknowledgement_List.pdf.

Funding

This project has received funding from the European Union's Horizon 2020 research and innovation program under grant agreement No. 666992 (LMA, NPO and DCA). LMA was partially supported by the National Institute Of Biomedical Imaging And Bioengineering of the National Institutes of Health under Award Number P41EB015922 and by the National Institute On Aging of the National Institutes of Health under Award Number P30AG066530. NPO is a UKRI Future Leaders Fellow (MRC MR/S03546X/1). This project was supported by the National Institute for Health Research University College London Hospitals Biomedical Research Centre. PAW was funded by a Medical Research Council Skills Development Fellowship (MR/T027770/1). ALY is supported by an MRC Skills Development Fellowship (MR/T027800/1). EPSRC grant EP/M020533/1 also supports this work. AA holds a Medical Research Council eMedLab Medical Bioinformatics Career Development Fellowship. This work was supported by the Medical Research Council (grant number MR/L016311/1: E-DADS). This work has received support from the EU-EFPIA Innovative Medicines Initiatives 2 Joint Undertaking (AMYPAD, grant No 115952). This joint undertaking receives support from the European Union's Horizon 2020 research and innovation program and EFPIA. This

communication reflects the views of the authors and neither IMI nor the European Union and EFPIA are liable for any use that may be made of the information contained herein. LEC has received research support by GE Healthcare (paid to institution).

Data collection and sharing for this project was funded by the Alzheimer's Disease Neuroimaging Initiative (ADNI) (National Institutes of Health Grant U01 AG024904) and DOD ADNI (Department of Defense award number W81XWH-12-2-0012). ADNI is funded by the National Institute on Aging, the National Institute of Biomedical Imaging and Bioengineering, and through generous contributions from the following: AbbVie, Alzheimer's Association; Alzheimer's Drug Discovery Foundation; Araclon Biotech; BioClinica, Inc.; Biogen; Bristol-Myers Squibb Company; CereSpir, Inc.; Cogstate; Eisai Inc.; Elan Pharmaceuticals, Inc.; Eli Lilly and Company; EuroImmun; F. Hoffmann-La Roche Ltd and its affiliated company Genentech, Inc.; Fujirebio; GE Healthcare; IXICO Ltd.; Janssen Alzheimer Immunotherapy Research & Development, LLC.; Johnson & Johnson Pharmaceutical Research & Development LLC.; Lumosity; Lundbeck; Merck & Co., Inc.; Meso Scale Diagnostics, LLC.; NeuroRx Research; Neurotrack Technologies; Novartis Pharmaceuticals Corporation; Pfizer Inc.; Piramal Imaging; Servier; Takeda Pharmaceutical Company; and Transition Therapeutics. The Canadian Institutes of Health Research is providing funds to support ADNI clinical sites in Canada. Private sector contributions are facilitated by the Foundation for the National Institutes of Health (www.fnih.org). The grantee organization is the Northern California Institute for Research and Education, and the study is coordinated by the Alzheimer's Therapeutic Research Institute at the University of Southern California. ADNI data are disseminated by the Laboratory for Neuro Imaging at the University of Southern California.

Competing interests

The authors report no competing interests.

Supplementary material

Supplementary material is available at *Brain* online.

References

1. Bloom, G. S. Amyloid-β and tau: the trigger and bullet in Alzheimer disease pathogenesis. *JAMA Neurol* **71**, 505–508 (2014).

2. Hardy, J. A. & Higgins, G. A. Alzheimer's disease: the amyloid cascade hypothesis. *Science* **256**, 184–185 (1992).

3. Selkoe, D. J. The molecular pathology of Alzheimer's disease. *Neuron* **6**, 487–498 (1991).

4. Braak, H. & Braak, E. Frequency of Stages of Alzheimer-Related Lesions in Different Age Categories. *Neurobiology of Aging* **18**, 351–357 (1997).

5. Braak, H., Thal, D. R., Ghebremedhin, E. & Del Tredici, K. Stages of the Pathologic Process in Alzheimer Disease: Age Categories From 1 to 100 Years. *Journal of Neuropathology & Experimental Neurology* **70**, 960–969 (2011).

6. Jacobs, H. I. L. *et al.* Structural tract alterations predict down-stream tau accumulation in amyloid positive older individuals. *Nat Neurosci* **21**, 424–431 (2018).

7. Palmqvist, S. *et al.* Earliest accumulation of β-amyloid occurs within the default-mode network and concurrently affects brain connectivity. *Nat Commun* **8**, 1214 (2017).

8. Collij, L. E. *et al.* Spatial-Temporal Patterns of β-Amyloid Accumulation: A Subtype and Stage Inference Model Analysis. *Neurology* **98**, e1692–e1703 (2022).

9. Jagust, W. Imaging the evolution and pathophysiology of Alzheimer disease. *Nat Rev Neurosci* **19**, 687–700 (2018).

10. Duyckaerts, C. *et al.* PART is part of Alzheimer disease. *Acta Neuropathol.* **129**, 749–756 (2015).

11. Coomans, E. M. *et al.* Genetically identical twins show comparable tau PET load and spatial distribution. *Brain* **145**, 3571–3581 (2022).

12. Schöll, M. *et al.* PET Imaging of Tau Deposition in the Aging Human Brain. *Neuron* **89**, 971–982 (2016).

13. Young, A. L. *et al.* Uncovering the heterogeneity and temporal complexity of neurodegenerative diseases with Subtype and Stage Inference. *Nature Communications* **9**, 4273 (2018).

14. Vogel, J. W. *et al.* Four distinct trajectories of tau deposition identified in Alzheimer's disease. *Nature Medicine* 1–11 (2021) doi:10.1038/s41591-021-01309-6.

15. Crary, J. F. *et al.* Primary age-related tauopathy (PART): a common pathology associated with human aging. *Acta Neuropathol* **128**, 755–766 (2014).

16. Bennett, D. A. *et al.* Religious Orders Study and Rush Memory and Aging Project. *J Alzheimers Dis* **64**, S161–S189 (2018).

17. McKhann, G. *et al.* Clinical diagnosis of Alzheimer's disease Report of the NINCDS-ADRDA Work Group* under the auspices of Department of Health and Human Services Task Force on Alzheimer's Disease. *Neurology* **34**, 939–939 (1984).

18. Consensus Recommendations for the Postmortem Diagnosis of Alzheimer's Disease. *Neurobiology of Aging* **18**, S1–S2 (1997).

19. Mirra, S. S. *et al.* The Consortium to Establish a Registry for Alzheimer's Disease (CERAD). Part II. Standardization of the neuropathologic assessment of Alzheimer's disease. *Neurology* **41**, 479–486 (1991).

20. Braak, H. & Braak, E. Neuropathological stageing of Alzheimer-related changes. *Acta Neuropathol* **82**, 239–259 (1991).

21. Crane, P. K. *et al.* Development and assessment of a composite score for memory in the Alzheimer's Disease Neuroimaging Initiative (ADNI). *Brain Imaging Behav* **6**, 502–516 (2012).

22. Gibbons, L. E. *et al.* A composite score for executive functioning, validated in Alzheimer's Disease Neuroimaging Initiative (ADNI) participants with baseline mild cognitive impairment. *Brain Imaging Behav* **6**, 517–527 (2012).

23. Young, A. L. *et al.* Ordinal SuStaIn: Subtype and Stage Inference for Clinical Scores, Visual Ratings, and Other Ordinal Data. *Frontiers in Artificial Intelligence* **4**, 111 (2021).

24. Young, A. L. *et al.* Data-driven neuropathological staging and subtyping of TDP-43 proteinopathies. 2023.01.31.23285242 Preprint at https://doi.org/10.1101/2023.01.31.23285242 (2023).

25. Aksman, L. M. *et al.* pySuStaIn: A Python implementation of the Subtype and Stage Inference algorithm. *SoftwareX* **16**, 100811 (2021).

26. Landau, S. & Jagust, W. Florbetapir processing methods. (2015).

27. Landau, S. & Jagust, W. Flortaucipir (AV-1451) processing methods. (2020).

28. Baker, S. L., Maass, A. & Jagust, W. J. Considerations and code for partial volume correcting [18F]-AV-1451 tau PET data. *Data in Brief* **15**, 648–657 (2017).

29. Landau, S. M. *et al.* Measurement of Longitudinal β-Amyloid Change with 18F-Florbetapir PET and Standardized Uptake Value Ratios. *J Nucl Med* **56**, 567–574 (2015).

30. Maass, A. *et al.* Comparison of multiple tau-PET measures as biomarkers in aging and Alzheimer's disease. *NeuroImage* **157**, 448–463 (2017).

31. Landau, S. M. *et al.* Amyloid Deposition, Hypometabolism, and Longitudinal Cognitive Decline. *Ann Neurol* **72**, 578–586 (2012).

32. Landau, S. M. *et al.* Comparing positron emission tomography imaging and cerebrospinal fluid measurements of β-amyloid. *Ann Neurol* **74**, 826–836 (2013).

33. Lewczuk, P., Lelental, N., Spitzer, P., Maler, J. M. & Kornhuber, J. Amyloid-β 42/40 cerebrospinal fluid concentration ratio in the diagnostics of Alzheimer's disease: validation of two novel assays. *J Alzheimers Dis* **43**, 183–191 (2015).

34. Bennett, D. A. *et al.* Overview and Findings from the Rush Memory and Aging Project. *Curr Alzheimer Res* **9**, 646–663 (2012).

35. Jack, C. R. *et al.* Longitudinal tau PET in ageing and Alzheimer's disease. *Brain* **141**, 1517–1528 (2018).

36. Lowe, V. J. *et al.* Widespread brain tau and its association with ageing, Braak stage and Alzheimer's dementia. *Brain* **141**, 271–287 (2018).

37. Busche, M. A. & Hyman, B. T. Synergy between amyloid-β and tau in Alzheimer's disease. *Nat Neurosci* **23**, 1183–1193 (2020).

38. Monsell, S. E. *et al.* Comparison of symptomatic and asymptomatic persons with Alzheimer disease neuropathology. *Neurology* **80**, 2121–2129 (2013).

39. Wuestefeld, A. *et al.* Age-related and amyloid-beta-independent tau deposition and its downstream effects. *Brain* awad135 (2023) doi:10.1093/brain/awad135.

40. Harold, D. *et al.* Genome-wide association study identifies variants at CLU and PICALM associated with Alzheimer's disease, and shows evidence for additional susceptibility genes. *Nat Genet* **41**, 1088–1093 (2009).

41. Lambert, J.-C. *et al.* Genome-wide association study identifies variants at CLU and CR1 associated with Alzheimer's disease. *Nat Genet* **41**, 1094–1099 (2009).

42. Myers, R. H. *et al.* Apolipoprotein E epsilon4 association with dementia in a population-based study: The Framingham study. *Neurology* **46**, 673–677 (1996).

43. Slooter, A. J. C. *et al.* Risk Estimates of Dementia by Apolipoprotein E Genotypes From a Population-Based Incidence Study: The Rotterdam Study. *Archives of Neurology* **55**, 964–968 (1998).

44. Insel, P. S., Hansson, O. & Mattsson-Carlgren, N. Association Between Apolipoprotein E ε2 vs ε4, Age, and β-Amyloid in Adults Without Cognitive Impairment. *JAMA Neurology* **78**, 229–235 (2021).

45. Strikwerda-Brown, C. *et al.* Association of Elevated Amyloid and Tau Positron Emission Tomography Signal With Near-Term Development of Alzheimer Disease Symptoms in Older Adults Without Cognitive Impairment. *JAMA Neurology* **79**, 975–985 (2022).

46. Ossenkoppele, R. *et al.* Amyloid and tau PET-positive cognitively unimpaired individuals are at high risk for future cognitive decline. *Nat Med* **28**, 2381–2387 (2022).

47. Livingston, G. *et al.* Dementia prevention, intervention, and care: 2020 report of the Lancet Commission. *The Lancet* **396**, 413–446 (2020).

48. Crary, J. F. Primary age-related tauopathy and the amyloid cascade hypothesis: the exception that proves the rule? *J Neurol Neuromedicine* **1**, 53–57 (2016).

49. Jellinger, K. A. *et al.* PART, a distinct tauopathy, different from classical sporadic Alzheimer disease. *Acta Neuropathol* **129**, 757–762 (2015).

50. Bell, W. R. *et al.* Neuropathologic, genetic, and longitudinal cognitive profiles in primary age-related tauopathy (PART) and Alzheimer's disease. *Alzheimers Dement* **15**, 8–16 (2019).

51. Frisoni, G. B. *et al.* The probabilistic model of Alzheimer disease: the amyloid hypothesis revised. *Nat Rev Neurosci* **23**, 53–66 (2022).

52. Yoon, B. *et al.* Abnormal tau in amyloid PET negative individuals. *Neurobiology of Aging* **109**, 125–134 (2022).

53. Murray, M. E. *et al.* Neuropathologically defined subtypes of Alzheimer's disease with distinct clinical characteristics: a retrospective study. *The Lancet Neurology* **10**, 785–796 (2011).

54. Vogel, J. W. & Hansson, O. Subtypes of Alzheimer's disease: questions, controversy, and meaning. *Trends in Neurosciences* **45**, 342–345 (2022).

55. Weiner, M. W. *et al.* Increasing participant diversity in AD research: Plans for digital screening, blood testing, and a community-engaged approach in the Alzheimer's Disease Neuroimaging Initiative 4. *Alzheimer's & Dementia* **19**, 307–317 (2023).

56. Young, A. L., Aksman, L. M., Alexander, D. C. & Wijeratne, P. A. Subtype and Stage Inference with Timescales. in *Information Processing in Medical Imaging* (eds. Frangi, A., de Bruijne, M., Wassermann, D. & Navab, N.) 15–26 (Springer Nature Switzerland, 2023). doi:10.1007/978-3-031-34048-2_2.

Figure legends

Figure 1 Positional variance diagrams (PVDs) for 2-subtype SuStaIn models. Each panel represents a subtype, i.e. a unique pattern of disease progression from early to late stage disease. **A**, **B**: PVDs for 2-subtype model trained on trained on ROSMAP's neuropathology data. Part **A** is the 'amyloid-first' subtype, **B** is the 'tau-first' subtype. **C, D:** PVDs for 2-subtype model trained on ADNI's amyloid and tau PET SUVR data. Part **C** is the 'amyloid-first' subtype, **D** is the 'tau-first' subtype. Each colored box represents the degree of certainty that a given regional marker (y-axis) has reached a given severity stage (in increasing order: red, purple or blue) at a given SuStaIn stage (x-axis).

Figure 2 Differences in Aβ and tau measures across early stage groups. Top row: pathology measures across early stage groups in the neuropathology analysis. **A, B:** raw Aβ plaque measures (percentage of region) in the angular gyrus and midfrontal regions, showing the expected increase in Aβ plaques in the two early amyloid-first groups (APOE ε4-, ε4+) with reference lines based on average values of those diagnosed as possible, probable and definite AD based on CERAD scoring of neuritic plaques. **C, D:** raw tangle density measures (per mm^2) in the entorhinal and hippocampal regions, showing the expected increase in the two early tau-first groups with reference lines based on average values of those assigned Braak I-VI stages. **Bottom row:** biomarker measures across early stage groups in the PET-based analysis. **E:** amyloid PET global SUVR, showing expected increase in both early amyloid-first groups and a small increase in early tau-first group (ε4-). Reference line: amyloid PET positivity threshold of 1.11 or greater. **F:** CSF Aβ-42/Aβ-40 ratio, showing decreased ratio (increased Aβ deposition) in early amyloid-first (ε4+) group relative to both early amyloid-first (ε4-) and stage-zero groups. Reference line: CSF Aβ-42/Aβ-40 ratio positivity threshold of 0.06 or less. **G:** tau PET entorhinal region SUVR, showing expected increase in tau pathology in both early tau-first groups. Reference line: regional positivity threshold of 1.2 or greater. **H:** CSF pTau, showing small increase in early amyloid-first (ε4+). Reference line: positivity threshold of 21 or greater.

Figure 3 Demographic measures across early stage groups along with a comparison of proportion of each group within APOE ε4+ and ε4- participants. Top row: ROSMAP neuropathology analysis, showing **A:** no differences in age between groups; **B:** early amyloid-first (ε4+) group has a higher proportion of females than the stage-zero group; **C:** small increase in years of education in early amyloid-first (ε4+) versus early amyloid-first (ε4-) group; and **D:** higher prevalence of early amyloid-first group within ε4+ participants. **Bottom row:** ADNI PET-based analysis, showing **E:** small increase in age in early tau-first (ε4+) group relative to stage-zero group; **F:** higher proportion of females in early tau-first groups relative to stage-zero group; **G:** fewer years of education in the early tau-first (ε4+) group versus both early tau-first (ε4-) and stage-zero groups; and **H:** as in neuropathology analysis, a higher prevalence of early amyloid-first group within ε4+ participants.

Figure 4 Longitudinal consistency of PET-based model. On the left are spaghetti plots of participants with either amyloid-first (**A**; $n = 78$) or tau-first (**C**; $n = 47$) as their estimated baseline subtype, stratified by APOE ε4 status within each figure. Each participant's longitudinal stage progression is depicted as a connected line, with opposite colors and 'x' markers used for points where the follow-up subtype is not consistent with the baseline subtype. The dashed lines represent the early-stage cut-off for each subtype (amyloid-first: stage nine, tau-first: stage ten). On the right are confusion matrices built by comparing each participant's estimated baseline subtype to their estimated two-year follow-up subtype, stratified by APOE ε4 status (**B**: $n = 58$ ε4-, **D**: $n = 45$ ε4+).

Figure 5 Longitudinal amyloid and tau PET SUVR trajectories for early-stage groups in PET-based model based on linear mixed effects models. A: amyloid PET based global SUVR trajectories using composite reference region that is recommended for longitudinal analysis, with an abnormality cut-off of 0.78 as reference line; **B-D:** tau PET based Braak composite SUVR trajectories with empirically chosen abnormality cut-offs based on distributions presented in Supplementary Table 8 (1.3 for Braak I in **B**, 1.25 for Braak III/IV in **C**, 1.2 for Braak V/VI in **D**).

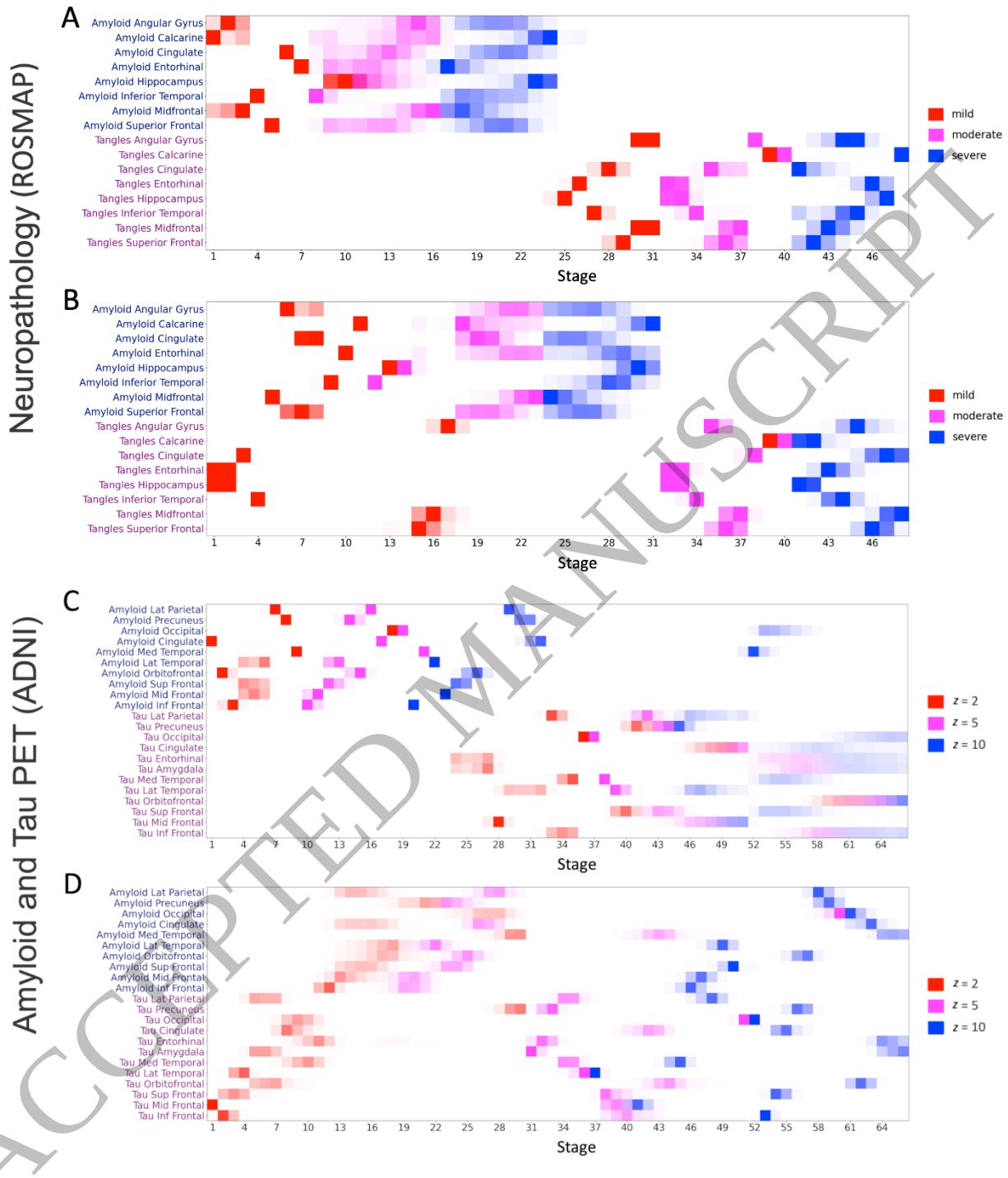

Figure 1
209x240 mm (x DPI)

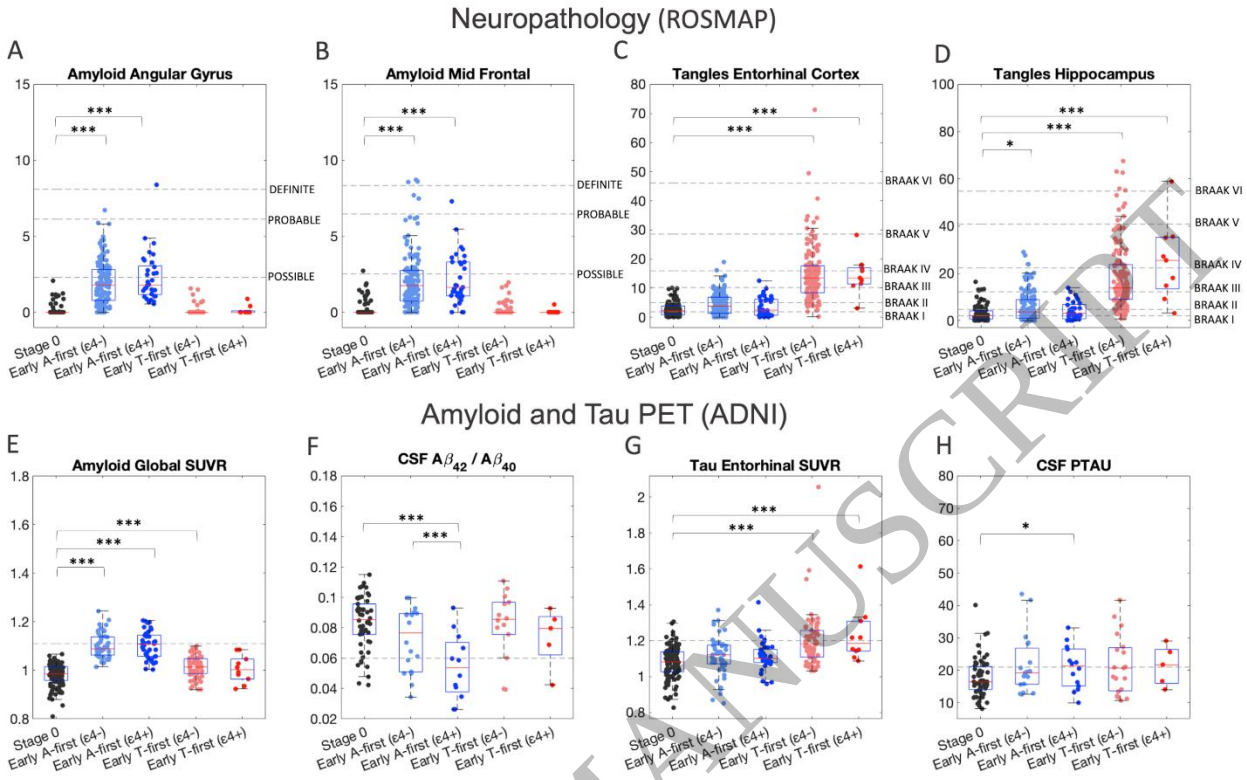

Figure 2
239x156 mm (x DPI)

1

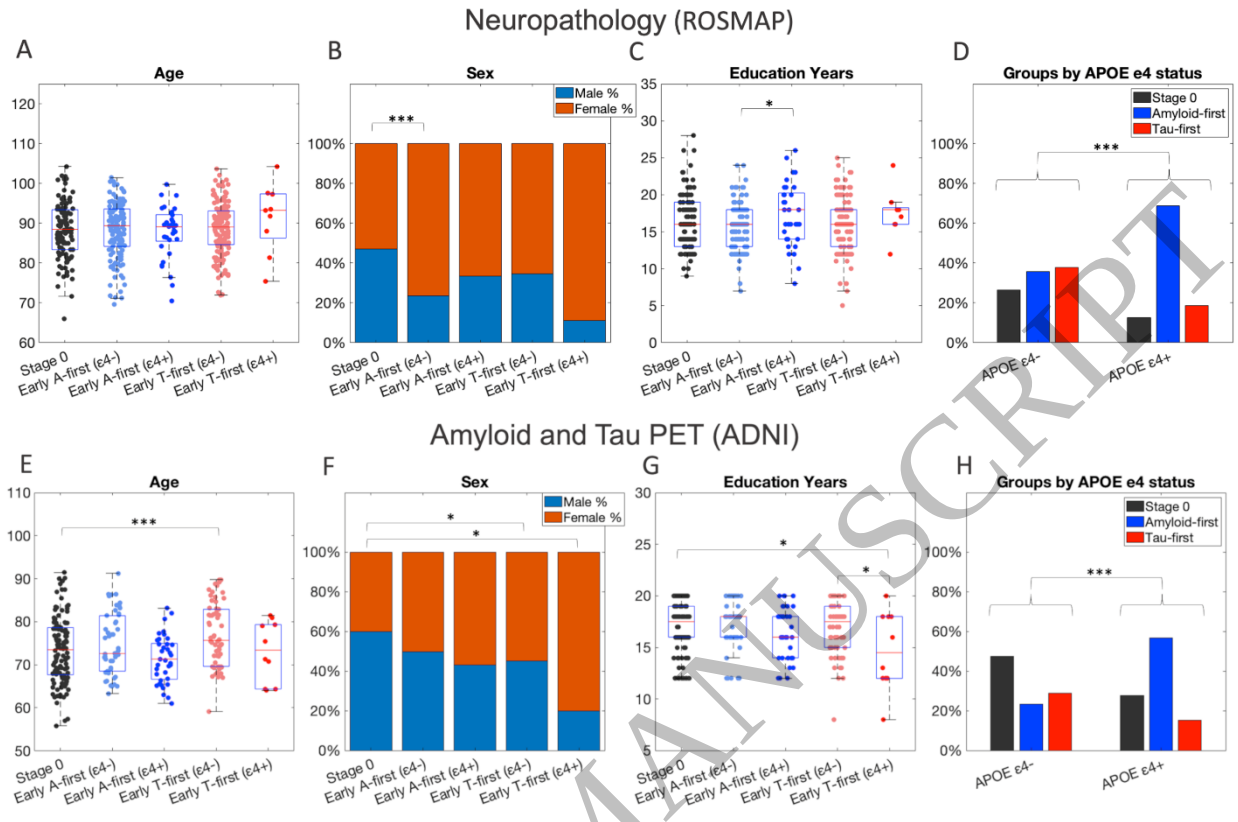

Figure 3
239x160 mm (x DPI)

1

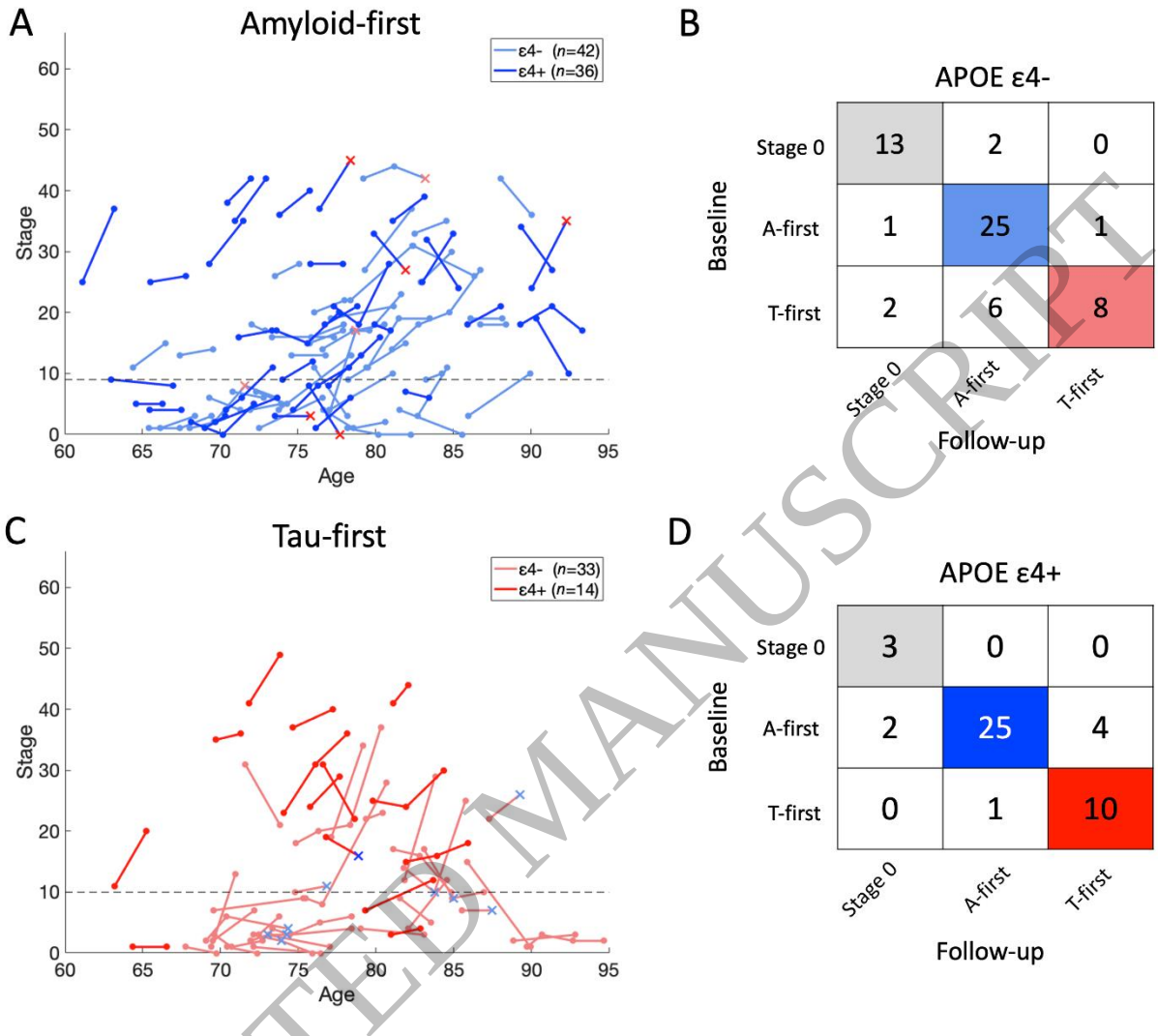

Figure 4
232x197 mm (x DPI)

1

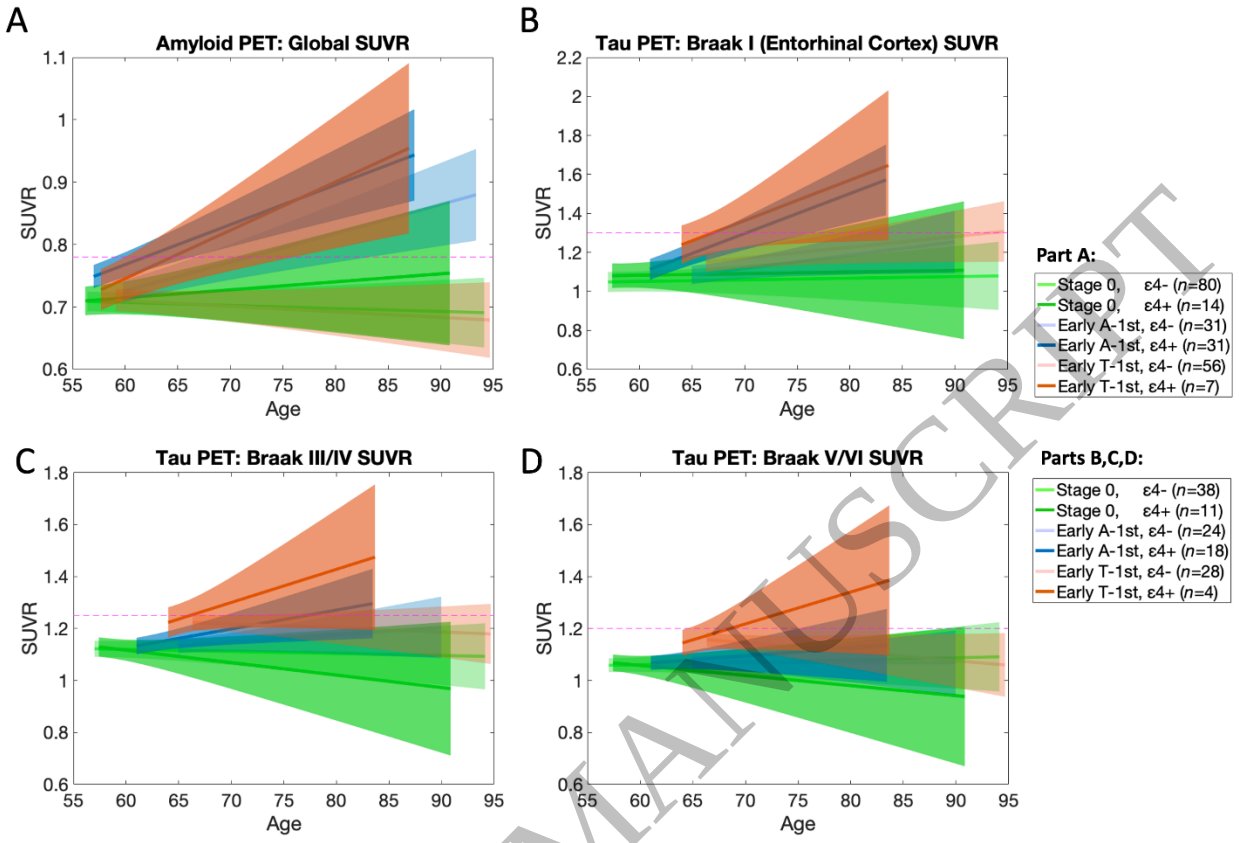

Figure 5
239x162 mm (x DPI)

Table 1 Characterization and comparison of subtyping cohorts

	ROSMAP	ADNI	
n	1338	502	
Age, Mean ± SD, [Min Max]	89.9 ± 6.4, [65.9 108.3]	75.2 ± 7.9, [55.3 93.8]	$<1 \times 10^{-6}$ ***
Education Years, Mean ± SD, [Min Max]	15.9 ± 3.6, [3.0 30.0]	16.4 ± 2.6, [8.0 20.0]	0.005**
Females, Percentage	69%	50%	$<1 \times 10^{-6}$ ***
APOE ε4 alleles (% 0,1,2)	76%, 22%, 2%	65%, 28%, 7%	$<1 \times 10^{-6}$ ***

APOE ε4 was available for all ROSMAP participants and 470 ADNI participants. We compared age and education years via one-way ANOVAs and sex and APOE ε4 carriage via chi-squared tests. SD = standard deviation. *P*-values of these tests are reported in right-hand column. * $P < 0.05$, ** $P < 0.01$, *** $P < 0.001$.